Journal of Alloys and Compounds 511 (2012) 101–106

Contents lists available at SciVerse ScienceDirect

Journal of Alloys and Compounds

journal homepage: www.elsevier.com/locate/jallcom

Synthesis and characterization of *in situ* carbon-coated Li_2FeSiO_4 cathode materials for lithium ion battery

Zipeng Yan, Shu Cai*, Lijuan Miao, Xing Zhou, Yongming Zhao

Key Laboratory for Advanced Ceramics and Machining Technology of Ministry of Education, Tianjin University, Tianjin 300072, People's Republic of China, China

ARTICLE INFO

Article history:
Received 27 July 2011
Received in revised form 26 August 2011
Accepted 30 August 2011
Available online 10 September 2011

Keywords:
Li_2FeSiO_4
Cathode material
Sol–gel method
Carbon coating
Lithium ion battery

ABSTRACT

Li_2FeSiO_4/C composites with *in situ* carbon coating were synthesized via sol–gel method based on acid-catalyzed hydrolysis/condensation of tetraethoxysilane (TEOS) with sucrose and L-ascorbic acid as carbon additives, respectively. As-obtained Li_2FeSiO_4/C composites prepared with L-ascorbic acid as a carbon additive are composed of nanoparticulate Li_2FeSiO_4 in an intimate contact with a continuous thin layer of residual carbon and exhibit large specific surface area up to 395.7 $m^2 g^{-1}$. The results indicate that structure of the residual carbon is graphene-rich with obviously lower disordered/graphene (D/G) ratio. These as-obtained Li_2FeSiO_4/C composites exhibit first discharge capacity of 135.3 mAh g^{-1} at C/16 and perform cycling stability, which are superior to those of Li_2FeSiO_4/C composites synthesized with sucrose as a carbon additive.

1. Introduction

Rechargeable lithium ion batteries are key components of the portable, entertainment, computing and telecommunication equipment required by today's information-rich, mobile society, due to their high energy density and design flexibility [1]. Compared with conventional lithium transition metal oxides as cathode materials for lithium ion batteries (e.g., $LiMn_2O_4$, $LiCoO_2$, and $LiNiO_2$), polyanion compounds with $(XO_4)^{n-}$ group (X = P, Si, Ge, etc.), have been extensively investigated owing to their higher safety and lower cost, in spite of their intrinsic low electronic conductivity and slow lithium ion diffusion. A successful example is $LiFePO_4$ [2], whose stability is rooted in a strong covalent P–O bond, hence superior electrochemical performance. During the further exploration of safe and cheap, but low conductivity materials, orthosilicate with a polyanionic framework is considered to be a kind of potential cathode material for next-generation lithium ion batteries.

Li_2FeSiO_4, first proposed by Nyten and co-workers [3], possesses a stronger Si–O bond in comparison to P–O bond, which is expected to translate into a higher chemical and electrochemical stability and thus a better cycle performance. However, just like $LiFePO_4$, Li_2FeSiO_4 also suffers from the problems of poor electronic conductivity and slow lithium ion diffusion, which has become a huge obstacle to its extensive application, especially in electric vehicles, and hybrid electric vehicles [4–6]. In the past few years, strategies to increase the low rate performance of bulk Li_2FeSiO_4 mainly focused on improving electron transport in the bulk or at the surface of the material, or on reducing the path length over which the electron and lithium ion have to move by using nano-sized materials [4–7]. Among the efforts, carbon coating is an effective way to enhance the electrochemical performance, for carbon can suppress the particle growth in the process of calcination and reduce Fe^{3+} to Fe^{2+}, thus ensuring the high purity of the products [7]. Additionally, adjusting the morphology or microstructure of Li_2FeSiO_4 to obtain porous and high specific surface area material constitutes another effective route to enhance the electrochemical performance [8].

As known, the selection of the carbon additive and the carbon mixing recipe are very important for tailoring the final properties of carbon-coated composite powders [9]. In previous studies, carbon additive sucrose was always mixed with the pre-synthesized Li_2FeSiO_4 precursor by ball milling process [6,10]. The resultant Li_2FeSiO_4/C composites were composed of Fe_3O_4 impurity, most likely, because the postaddition of sucrose is not favorable for homogeneous mixing of raw materials. In this study, we design a sol–gel method for synthesis of *in situ* carbon-coated Li_2FeSiO_4. Tetraethoxysilane (TEOS), which was extensively studied for the synthesis of monolithic silica column finding its use in the electrochromatography, could be catalyzed by acid (e.g., hydrochloric acid) or alkali (e.g., dodecylamine) [11]. Therefore, a facile sol–gel method based on acid-catalyzed hydrolysis/condensation of TEOS was introduced for the preparation of Li_2FeSiO_4/C. Sucrose was added to the starting material in the synthesis of the precursor, through which the molecular-level mixing of the starting ingredients could be achieved. To the best of our knowledge, L-ascorbic

* Corresponding author.
E-mail address: caishu@tju.edu.cn (S. Cai).

0925-8388/$ – see front matter © 2011 Elsevier B.V. All rights reserved.
doi:10.1016/j.jallcom.2011.08.095

acid was first employed as carbon additive in the synthesis of Li_2FeSiO_4/C, whereby graphene-rich carbon was coated uniformly on the surface of the particles, of which the mechanism was also discussed in this paper. The effects of carbon additives (i.e., L-ascorbic acid and sucrose) on the structural and electrochemical characteristics of the Li_2FeSiO_4/C were investigated comparatively.

2. Experimental

2.1. Synthesis of Li_2FeSiO_4/C

Li_2FeSiO_4/C was prepared by a sol–gel method based on acid-catalyzed hydrolysis/condensation of TEOS. All starting materials are soluble in de-ionized water or ethanol, and no phase separation appears before condensation reaction, for the purpose of a homogeneous precursor. Ethanol is considered to be good solvent for its lower surface tension compared with water, leading to a weaker capillary force and thus better dispersion of the particles. When employing ethanol as the solvent to prepare Sample-S, however, the homogeneous gel was not successfully synthesized, presumably because the existence of sucrose was detrimental to the condensation of TEOS under the applied condition. To address this problem, we tried to employ water as solvent and thereby HNO_3 to promote the hydrolysis of the TEOS in water. In the case of Li_2FeSiO_4/C employing sucrose as carbon additive (named as Sample-S), 1.8 ml of TEOS was mixed with 7.4 ml of de-ionized water and 0.6 ml of 2 M HNO_3 and hydrolyzed for 30 min under magnetic stirring. Then the lithium acetate dihydrate, iron (III) nitrate nonahydrate and 0.705 g of sucrose powders were added to TEOS water mixture, respectively, and reactants were stirred for 3 h at room temperature. After the reaction, the clear solution was transferred into a Teflon-lined stainless-steal autoclave, sealed, and maintained at 120 °C for 20 h, during which condensation occurred. The resulting brown wet gel precursor was dried at 80 °C.

In the preparation of Li_2FeSiO_4/C employing L-ascorbic acid as carbon source (named as Sample-A), 1.8 ml of TEOS was added to 15 ml of ethanol under magnetic stirring, followed by the addition of 0.3 ml of acetic acid. Separately lithium acetate dihydrate and iron (III) nitrate nonahydrate were dissolved in TEOS ethanol mixture and the obtained mixture was thoroughly stirred for 3 h at room temperature. Finally, 1.057 g of L-ascorbic acid dissolved in a minimal amount of de-ionized water, and the prepared solution were mixed together quickly and transferred into a Teflon-lined stainless-steal autoclave, sealed, and maintained at 120 °C for 20 h, during which condensation occurred. The resulting black wet gel precursor was dried at 60 °C.

After thorough grinding with a mortar and pestle, the obtained xerogels were pelleted and calcined in a gas-tight quartz tube with a constant flow of N_2 gas. The initial heating rate was 10 °C min^{-1}. After reaching 650 °C, the samples were maintained at that temperature for 10 h and then left to cool down to room temperature.

2.2. Measurements

The crystallographic structural characterization was performed by X-ray powder diffraction (XRD, Rigaku D/max 2500) employing Cu Kα radiation (40 kV/200 mA). An integrated Raman microscope system (LabRAM HR, HORIBA Jobin Yvon) was used to analyze the structure of the carbon layer. Scanning electron microscopy (SEM) imaging was carried on FE-SEM (HITACHI S-4800). The nature and thickness of the carbon coating was observed with high-resolution transmission electron microscope (HR-TEM, Philips Tecnai G2 F20). The specific surface area was computed from N_2 sorption data (Quantachrome NOVA) using the Brunauer–Emmett–Teller (BET) method. The carbon content was calculated from thermogravimetric data (TG, NETZSCH STA 449C). The sample was heated from 35 °C to 600 °C in air at a rate of 10 °C min^{-1}.

Electrochemical characterization was performed using CR2430 coin-type cell. The cathode electrode was prepared by dispersing 85 wt.% active powders, 15 wt.% acetylene black, and 5 wt.% polyfluortetraethylene (PTFE) in ethanol to form a paste. Then the paste was rolled to a thin film and cut into circular discs as the cathodes. These electrode discs were assembled in coin cells in an argon-filled glove box, with lithium metal as the negative electrode separated by a Celgard 2400 separator. The electrolyte used was 1 mol l^{-1} $LiPF_6$ in EC:DMC:DEC (1:1:1 ratio by volume). Galvanostatic charge/discharge measurements were performed between 1.5 and 4.8 V (vs. Li/Li^+) at 25 °C by the Neware battery testing system. Electrochemical impedance spectroscopy (EIS) was measured at 25 °C using a CHI 660 electrochemical instrument in the frequency range 100 kHz to 0.1 Hz, with an AC voltage of 5 mV.

3. Results and discussion

The X-ray diffraction patterns of the as-synthesized powders heat treated at 650 °C for 10 h are shown in Fig. 1. The main diffraction peaks of both samples are in good agreement with the previous report by Nishimura et al. [12]. Then we identified it as Li_2FeSiO_4 phase on the basis of a monoclinic structure with the space group

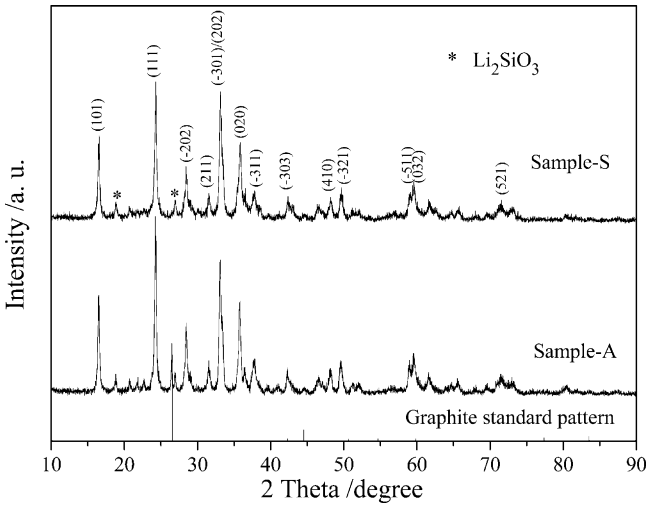

Fig. 1. XRD patterns of Li_2FeSiO_4/C composites and graphite standard pattern.

of $P2_1$. A little Li_2SiO_3 impurity was detected in both samples. It was considered that Fe^{3+} (e.g., Fe_2O_3) impurities existed in both samples in terms of the stoichiometric amounts of the reactants, despite the undetectable Fe^{3+} impurities peaks. The reasons for the absence of Fe^{3+} impurities peaks are their low crystallinity and their small amounts. The existence of Fe^{3+} impurities would not only be detrimental to the cycling performance [13], but also have an effect on the charge/discharge curves, which would be discussed later. No noticeable changes of the XRD patterns were observed for the carbon-coated Li_2FeSiO_4, suggesting that the Li_2FeSiO_4 structure was well maintained under our carbon coating experimental conditions. It is worth noting that in Sample-A, a main peak at 26.5° (2θ), together with several other relatively weak peaks, is corresponding well with the crystallized graphite (PDF# 65-6212), indicating that the formed carbon, generated from the L-ascorbic acid, was crystallized during the pyrolysis process. This XRD result is consistent with Huang's report of the Li_2FeSiO_4/carbon/carbon nano-tubes, obtained via a traditional solid-state reaction method employing multiwalled carbon nano-tubes as carbon additive [4]. Two reasons should be considered for the graphitization of the carbon additive L-ascorbic acid in the process of calcination. On one hand, carbon additive microstructure plays an important role in deciding the generated carbon structure [9,14]. Fig. 2 demonstrates the molecular structures of both carbon additives. As revealed, each molecule of L-ascorbic acid consists of an almost planar five-membered ring plus a side chain [15] (Fig. 2a). This kind of structure was readily to transform to graphite with a sheet like structure where the atoms all lie in a plane, in view of the principle of lowest energy [14,16]. Therefore, L-ascorbic acid may act as a template for the formation of graphite precursor upon heating. On the other hand, iron nitrate, which was regarded as one kind of graphitization catalysts, most likely catalyzed the conversion of L-ascorbic acid to the graphite in the Li_2FeSiO_4/C composites [16–18]. The catalytic graphitization is believed to involve dissolution of carbon in the catalyst or formation of carbide to precipitate graphite, lowering the graphitization temperature [19]. Similar graphitization process was also corroborated by Doeff et al., who employed iron nitrate graphitization catalyst in addition to pyromellitic acid during the final calcination step, whereby graphite-rich carbon was obtained to coat $LiFePO_4$ [16,17]. As for Sample-S, no evidence of diffraction peaks for graphite appears in the diffraction patterns, presumably because the graphitization catalyst made no difference in the transformation of sucrose to crystallized graphite during the calcination process, and thus the pyrolysis of sucrose produced carbons

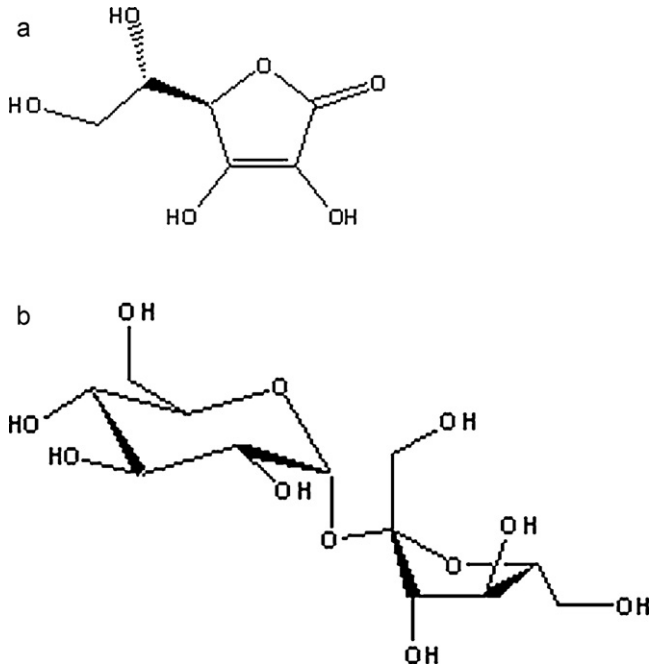

Fig. 2. Molecular structures of the carbon additives. (a) L-Ascorbic acid and (b) sucrose.

exhibiting tangled geometric arrangement of the crystallites that prevented further crystal growth even at high temperatures.

To gain additional insight into the nature of the carbon coating layer on the particles surface, we studied the structure of the cathode surface with micro-Raman spectroscopy (Fig. 3). Since the penetration depth of the light inside the Li_2FeSiO_4/C particles in Raman scattering is very small, this technique is a probe of the first layers at the surface of coated particles, and allows the detection of carbon coating. Two intense broad bands located at ~1345 and ~1590 cm^{-1} dominated both spectra of the samples. The structure at 1590 cm^{-1} mainly corresponds to the G line associated with the optically allowed E_{2g} zone center mode of crystalline graphite, the structure at 1345 cm^{-1} mainly corresponds to the D line associated with disorder-allowed zone-edge modes of graphite. The calculated integrated Raman intensity ratios of I_D/I_G bands for Sample-S, Sample-A are 1.3 and 0.5, respectively. A low I_D/I_G ratio is an indication of the presence of larger amount of graphene as compared to the disordered carbon structure [17].

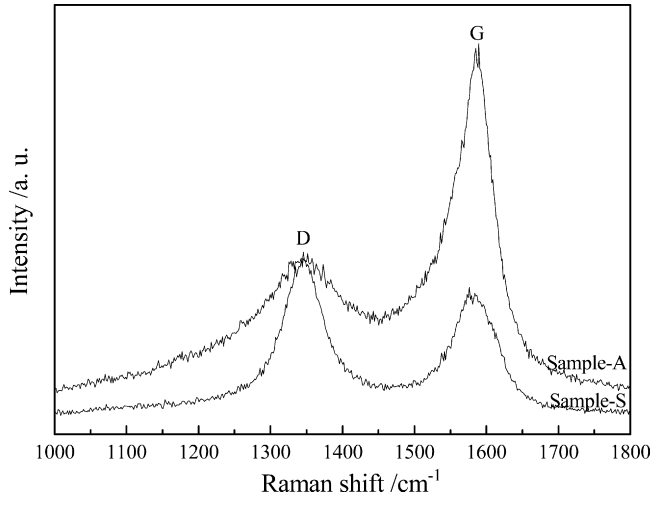

Fig. 3. Raman spectra of Li_2FeSiO_4/C samples.

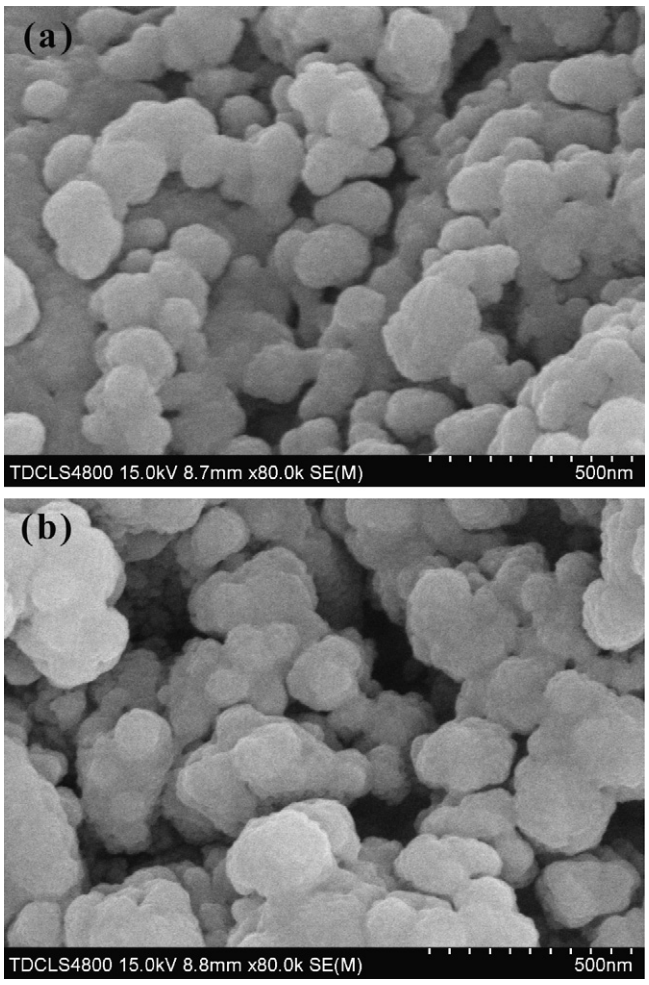

Fig. 4. SEM micrographs of Li_2FeSiO_4/C composites. (a) Sample-S and (b) Sample-A.

It is believed that the electronic conductivity of Li_2FeSiO_4/C composites is a strong function not only of the amount of carbon but of its structure (in particular, disordered/graphene ratios) and distribution [17,21]. The low value for the I_D/I_G indicates a high degree of graphitization. The increasing degree of graphitization can improve the electronic conductivity of residual carbon and thus provide better electronic contact between Li_2FeSiO_4/C particles with large agglomerates resulting in better electrochemical performance. In consequence, Sample-A is expected to exhibit distinctive electrochemical properties, due to the larger amount of graphene in the residual carbon.

The SEM micrographs (Fig. 4) show the spherical granules formed in the course of calcination. The surfaces of the particles are free of any crystal faceting, which could be further confirmed by the following HR-TEM images (Fig. 5a and b). This is directly attributable to the suppression of carbon coating in preferential growth of crystal grains in the process of calcination. A tendency towards agglomeration of primary particles can also be observed in both samples, in which the diameter of the primary particles ranges from ~50 to 100 nm for Sample-S (Fig. 4a), and ~75 to 150 nm for Sample-A (Fig. 4b), respectively, and shows a narrow particle size distribution. The pyrolysis of precursor, such as acetate, nitrate, as well as carbon additives, resulted in porous and agglomerated particles. With regards to the agglomeration distinction, the role of solvent properties should not be negligible because ethanol, employed as solvent in the preparation of Sample-A precursor, exhibits a lower surface tension compared with water, used as solvent in the synthesis of Sample-S precursor, leading to a

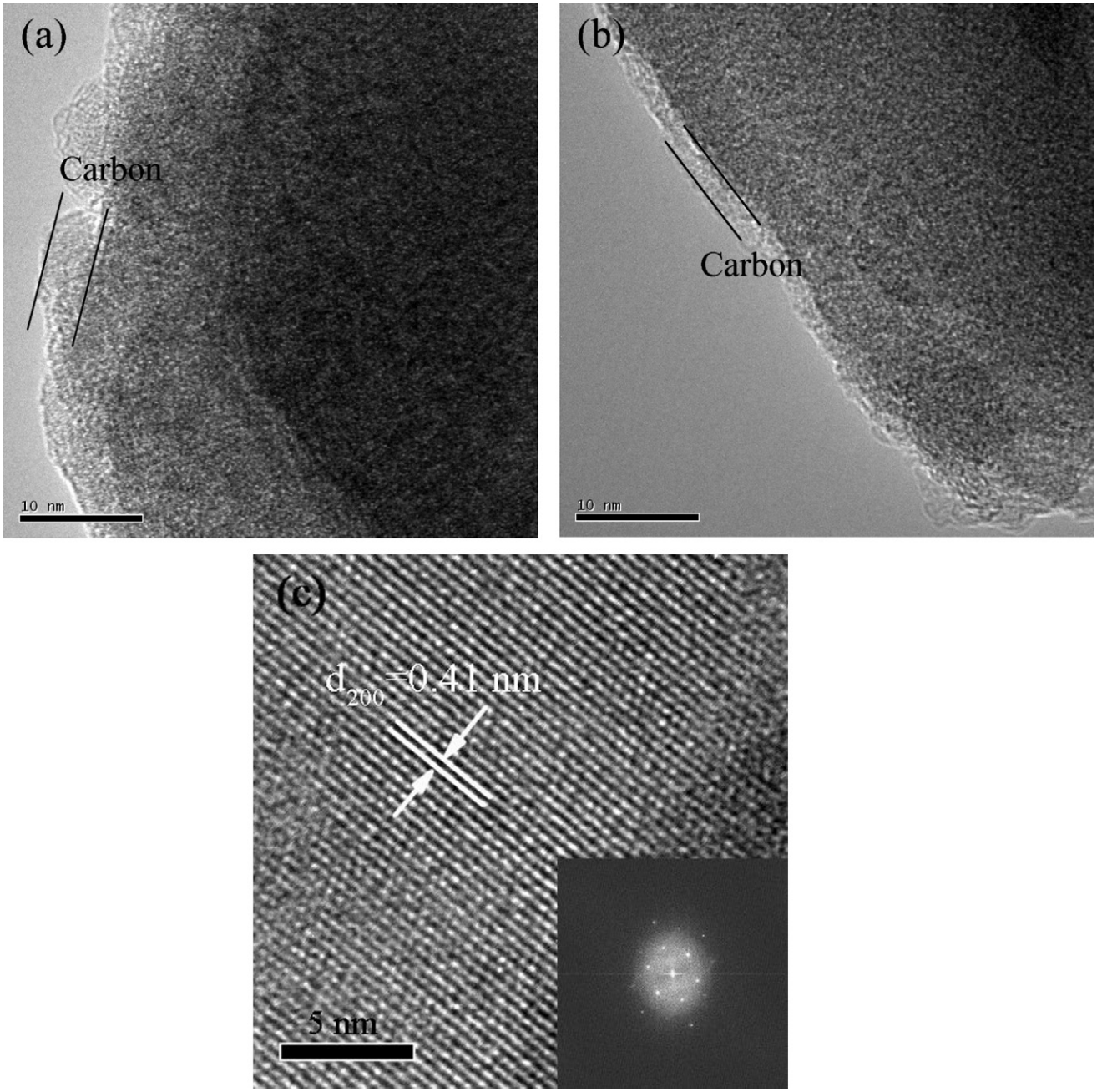

Fig. 5. HR-TEM images of Li_2FeSiO_4/C composites. (a) Sample-S, (b) Sample-A, and (c) body part of Li_2FeSiO_4 phase (the inset shows the corresponding FFT pattern).

weaker capillary force and thus better dispersion of the particles. The images of Sample-A reveals highly associated microstructure of the product with clearly visible macropores (~100 nm). BET surface area demonstrates that the specific surface area for Sample-S is 14.1 $m^2 g^{-1}$, while the corresponding value is 395.7 $m^2 g^{-1}$ for Sample-A. It is reported that the electrochemical properties are strongly affected by the specific surface area, and that samples with a larger specific surface area reveal better electrochemical performance, owing to short lithium ion diffusion pathway [8,20,22]. The porous structure of Sample-A contributes mainly to the higher specific surface area, in spite of slightly larger particle size, which will provide it with good electrochemical performance.

The HR-TEM images of the samples are shown in Fig. 5. It is observed that small particles are in an intimate contact with a continuous thin layer of conducting carbon. The carbon content in Li_2FeSiO_4/C composite is 7.8 wt.% for Sample-S and 7.1 wt.% for Sample-A, according to TG measurements. We believe that this layer was generated during the calcination process because of the carbonization of sucrose, L-ascorbic acid for Sample-S and Sample-A, respectively. Sample-A displayed a more uniform film whose thickness is ~2 nm around the particles. Poor cell lifetimes are rooted mainly in side reactions occurring at the electrode–electrolyte interface [1] (e.g., Li_2FeSiO_4 is degraded by the HF formed in the electrolyte by the hydrolysis of $LiPF_6$ [23]). Thus, a homogeneous coating of carbon minimizes the surface area of the active material in direct contact with the electrolyte, which is expected to inhibit, at least to a great extent, the side reactions between Li_2FeSiO_4 and the HF. The lattice fringes of the crystallized Li_2FeSiO_4 are ambiguous, due to the fact that Li_2FeSiO_4 is quite unstable when exposed to the electron beam [24]. Fig. 5c reveals the body part of the Li_2FeSiO_4 particle of Sample-A. The clear lattice fringes with interplannar distance of 4.1 Å is in accordance with the

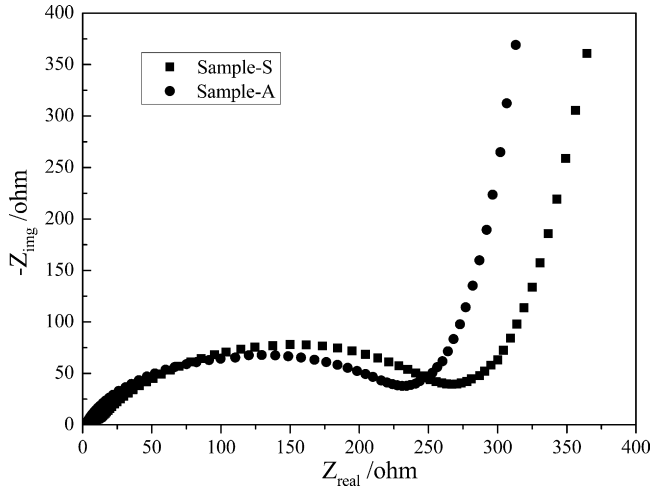

Fig. 6. Nyquist plots of Li_2FeSiO_4/C composites electrodes in the frequency range between 0.1 Hz and 100 kHz.

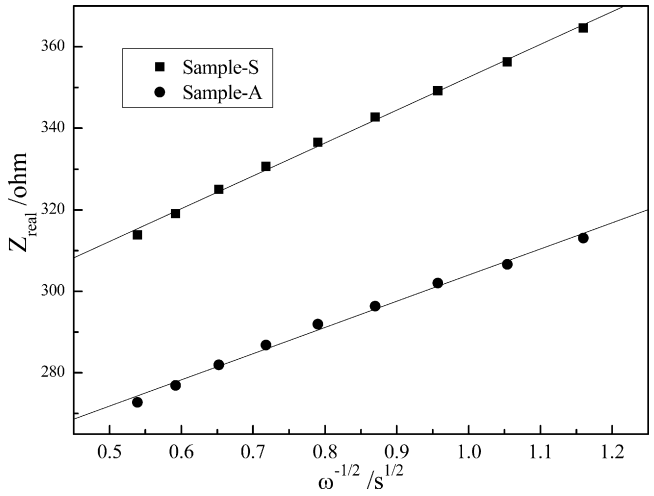

Fig. 7. The relationship between Z_{real} and $\omega^{-1/2}$ at low frequencies for Li_2FeSiO_4/C composites.

d-spacing of the (0 0 2) planes of Li_2FeSiO_4. The corresponding fast Fourier transform (FFT) pattern (the inset in Fig. 5c) of the body part can be indexed to diffraction spots for the Li_2FeSiO_4 phase, which is consistent with the powder XRD results.

Fig. 6 represents the impedance spectra of the Li_2FeSiO_4/C composites in the frequency range from 0.1 Hz to 100 kHz at fully discharge state at 25 °C. As shown, each Nyquist plot is composed of a depressed semicircle and an inclined line. Based on the literature [25], the intercept at the Z_{real} axis in high frequency corresponds to the ohmic resistance of the electrolyte and electrode (R_e). The semicircle in the middle frequency range indicates the charge transfer resistance (R_{ct}). The inclined line in the low frequency is closely correlated with the Warburg coefficient (σ_ω), which is associated with lithium ion diffusion. The diffusion coefficient values of the lithium ions (D_{Li}) can be obtained from Eq. (1):

$$D_{Li} = 0.5\left(\frac{RT}{An^2F^2\sigma_\infty C}\right) \quad (1)$$

where R is the gas constant, T is the absolute temperature, A is the surface area of the electrode, n is the number of electrons per molecule during oxidation, F is the Faraday constant, C is the concentration of lithium ion, σ_ω is the Warburg coefficient which is relative with Z_{real} obtained from Eq. (2):

$$Z_{real} = R_e + R_{ct} + \sigma_\omega \omega^{-1/2} \quad (2)$$

where ω is the angular frequency in the low frequency region. Both R_e and R_{ct} are kinetics parameters independent of frequency. So σ_ω is the slope for the plot of Z_{real} vs. the reciprocal square root of the lower angular frequencies ($\omega^{-1/2}$). Fig. 7 displays the linear fitting of Z_{real} vs. $\omega^{-1/2}$, from which the slope σ_ω can be obtained. All the parameters obtained and calculated from EIS are recorded in Table 1. It can be observed that Sample-A exhibits a lower charge transfer resistance and a higher lithium ion diffusion coefficient than those of Sample-S. Two points may account for the EIS results. One is the high specific surface area of Sample-A, which contributes to the improvement of the diffusion of lithium ions by means of shortening the lithium ion diffusion pathway and it also affects the kinetics of the liquid electrolyte. And the other point should be the thinner and more uniform carbon coating of Sample-A, which allows for smaller hindrance for lithium ions diffusion because the carbon coating network is an intrinsically inert material for lithium ion diffusion.

Table 1
Impedance parameters of Li_2FeSiO_4/C composites.

Samples	R_e (Ω)	R_{ct} (Ω)	σ_ω (Ω s$^{1/2}$)	D_{Li} (cm^2 s^{-1})
Sample-S	8.8	295	80.5	3.62E−13
Sample-A	2.9	255	64.2	1.35E−12

The second charge/discharge curves of samples with different rates between 1.5 and 4.8 V are presented in Fig. 8. At charge/discharge rates of C/16 and C/10, two samples did not show apparent variation. As the rate was increased to C/1, the differences between the two samples became pronounced. It is clear that Sample-A exhibits relatively smaller polarization loss and higher discharge capacity, in comparison with Sample-S. This could probably be attributed to the following reasons: at low rates (C/16, C/10), the effect of charge transfer resistance can be ignored. However, at higher rate (C/1), for which the supply of electrons becomes problematic and the charge transfer resistance plays an important role in the potential drop for the kinetics limitation, the advantages of high specific surface area are obviously revealed. High specific surface area facilitates the Lithium ions extraction/insertion, and accordingly elevates the high rate performance [4]. One may note that in the case of Sample-S, two discharge plateaus at ~3.0 and ~2.0 V could be found at different rates. This could be explained that the potential around 3.0 V is associated with the lithiation of $LiFeSiO_4$ phase, whereas the lower potential plateau around 2.0 V

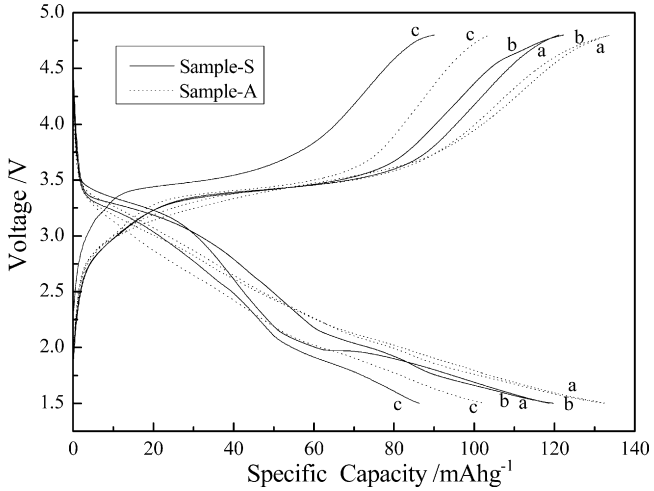

Fig. 8. Charge/discharge curves of samples in the voltage range of 1.5–4.8 V (vs. Li^+/Li) at different rates: (a) C/16, (b) C/10, and (c) C/1.

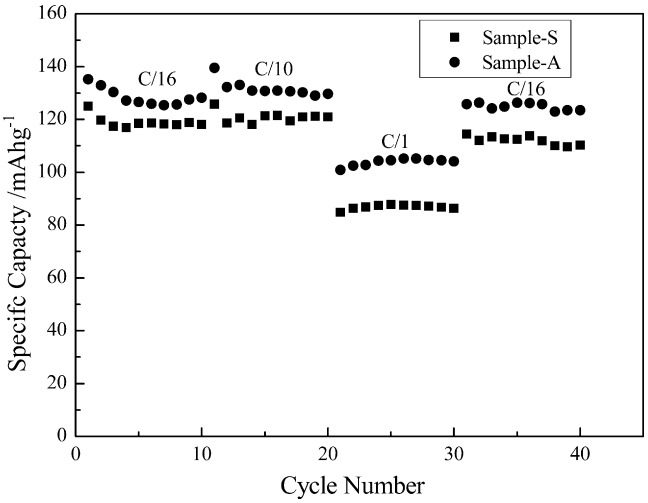

Fig. 9. Cycle performances of Li_2FeSiO_4/C samples at different rates.

probably originated from the lithiation process of Fe^{3+} (e.g., Fe_2O_3) impurities in the as-obtained Li_2FeSiO_4/C composites because the lithiation of Fe^{3+} impurities would have a direct bearing on the kinetics of thermodynamic stabilization, thus different equilibrium potentials measured during the redox process [26].

Fig. 9 reveals the cycle performance of both samples at different rates. The initial discharge capacity at the low current rate of C/16 is 135.3 mAh g^{-1} for Sample-A, while the corresponding value for Sample-S is 125.0 mAh g^{-1}. The capacity was calculated on the basis of as-synthesized samples, including the amount of *in situ* carbon. The discharge capacity of both samples decreases gradually during the first several cycles. The difference of capacity between both samples becomes more obvious when cycling at high rate (C/1). Therefore, the electrode prepared with Sample-A is superior to that of Sample-S in both the rate performance and cycling stability. This could be attributed to the fact that high specific surface area hence short lithium ion diffusion pathway, crystallized graphite constituting carbon coating thereby improving the electronic conductivity, and homogeneous coating of carbon thus minimizing the surface area of the active material in direct contact with the electrolyte.

4. Conclusion

Li_2FeSiO_4/C composites were successfully prepared by a facile sol–gel method in the present study. The effects of different carbon additives (i.e., L-ascorbic acid and sucrose) on the structural and electrochemical characteristics of the Li_2FeSiO_4/C were investigated comparatively. The *in situ* coating of carbon on the Li_2FeSiO_4 particles was formed by the pyrolysis of carbon additives during the calcination process. The composites, obtained via an ethanol-based sol–gel route employing L-ascorbic acid as carbon additive, exhibited a large specific surface area and porous nanostructure. Raman spectroscopy indicates that the structure of the residual carbon coated in this sample is of high degree of graphitization. Owing to the structure advantages, Li_2FeSiO_4/C composites prepared with L-ascorbic acid as carbon additive exhibited a higher electronic conductivity and lithium ion diffusion coefficient than those of Li_2FeSiO_4/C synthesized with sucrose, which, in turn, translated into better rate performance and cycling stability.

Acknowledgements

Authors acknowledge the financial support by China Natural Science Foundation (Grant Nos. 50772072, 51072129), Tianjin Natural Science Foundation (Grant No. 11JCYBJC02600).

References

[1] J.M. Tarascon, M. Armand, Nature 414 (2001) 359.
[2] A.K. Padhi, K.S. Nanjundaswamy, J.B. Goodenough, J. Electrochem. Soc. 144 (1997) 1188.
[3] A. Nyten, A. Abouimrane, M. Armand, T. Gustafsson, J.O. Thomas, Electrochem. Commun. 7 (2005) 156.
[4] X.B. Huang, X. Li, H.Y. Wang, Z.L. Pan, M.Z. Qu, Z.L. Yu, Electrochim. Acta 55 (2010) 7362.
[5] R. Dominko, J. Power Sources 184 (2008) 462.
[6] Z.L. Gong, Y.X. Li, G.N. He, J. Li, Y. Yang, Electrochem. Solid-State Lett. 11 (2008) A60.
[7] S. Zhang, C. Deng, S.Y. Yang, Electrochem. Solid-State Lett. 12 (2009) A136.
[8] X.Y. Fan, Y. Li, J.J. Wang, L. Gou, P. Zhao, D.L. Li, L. Huang, S.G. Sun, J. Alloys Compd. 493 (2010) 77.
[9] Y.H. Nien, J.R. Carey, J.S. Chen, J. Power Sources 193 (2009) 822.
[10] H.J. Guo, X. Cao, X.Q. Li, L.M. Li, X.H. Li, Z.X. Wang, W.J. Peng, Q.H. Li, Electrochim. Acta 55 (2010) 8036.
[11] L.J. Yan, Q.H. Zhang, W.B. Zhang, Y.Q. Feng, L.H. Zhang, T. Li, Y.K. Zhang, Electrophoresis 26 (2005) 2935.
[12] S. Nishimura, S. Hayase, R. Kanno, M. Yashima, N. Nakayama, A. Yamada, J. Am. Chem. Soc. 130 (2008) 13212.
[13] K. Zaghib, A. Mauger, F. Gendron, C.M. Julien, Solid State Ionics 179 (2008) 16.
[14] Y.Q. Hu, M.M. Doeff, R. Kostecki, R. Finones, J. Electrochem. Soc. 151 (2004) A1279.
[15] J. Hvoslef, Acta Crystallogr. B 24 (1968) 23.
[16] M.M. Doeff, J.D. Wilcox, R. Kostecki, G. Lau, J. Power Sources 163 (2006) 180.
[17] M.M. Doeff, J.D. Wilcox, R. Yu, A. Aumentado, M. Marcinek, R. Kostecki, J. Solid State Electrochem. 12 (2008) 995.
[18] C. Emmenegger, J.M. Bonard, P. Mauron, P. Sudan, A. Lepora, B. Grobety, A. Zuttel, L. Schlapbach, Carbon 41 (2003) 539.
[19] Y.G. Wang, Y. Korai, I. Mochida, K. Nagayama, H. Hatano, N. Fukuda, Carbon 39 (2001) 1627.
[20] J.K. Kim, J.W. Choi, G.S. Chauhan, J.H. Ahn, G.C. Hwang, J.B. Choi, H.J. Ahn, Electrochim. Acta 53 (2008) 8258.
[21] F.Y. Su, C.H. You, Y.B. He, W. Lv, W. Cui, F.M. Jin, B.H. Li, Q.H. Yang, F.Y. Kang, J. Mater. Chem. 20 (2010) 9644.
[22] M. Konarova, I. Taniguchi, J. Power Sources 195 (2010) 3661.
[23] D. Ensling, M. Stjerndahl, A. Nyten, T. Gustafsson, J.O. Thomas, J. Mater. Chem. 19 (2009) 82.
[24] R. Dominko, M. Bele, M. Gaberscek, A. Meden, M. Remskar, J. Jamnik, Electrochem. Commun. 8 (2006) 217.
[25] C. He, I.D. Raistrick, R.A. Huggins, J. Electrochem. Soc. 127 (1980) 343.
[26] C. Sirisopanaporn, C. Masquelier, P.G. Bruce, A.R. Armstrong, R. Dominko, J. Am. Chem. Soc. 133 (2011) 1263.